European Journal of Medicinal Chemistry 132 (2017) 262–273

Contents lists available at ScienceDirect

European Journal of Medicinal Chemistry

journal homepage: http://www.elsevier.com/locate/ejmech

Research paper

Anthranilamide-based 2-phenylcyclopropane-1-carboxamides, 1,1'-biphenyl-4-carboxamides and 1,1'-biphenyl-2-carboxamides: Synthesis biological evaluation and mechanism of action

Demetrio Raffa [a, *], Fabiana Plescia [a], Benedetta Maggio [a, **], Maria Valeria Raimondi [a], Antonella D'Anneo [b], Marianna Lauricella [c], Giuseppe Daidone [a]

[a] Department of Biological, Chemical and Pharmaceutical Sciences and Technologies, Medicinal Chemistry and Pharmaceutical Technologies Section, University of Palermo, Via Archirafi 32, 90123 Palermo, Italy
[b] Department of Biological, Chemical and Pharmaceutical Sciences and Technologies, Laboratory of Biochemistry, University of Palermo, 90127, Palermo, Italy
[c] Department of Experimental Biomedicine and Clinical Neurosciences, Laboratory of Biochemistry, University of Palermo, 90127, Palermo, Italy

ARTICLE INFO

Article history:
Received 3 November 2016
Received in revised form
21 March 2017
Accepted 23 March 2017
Available online 24 March 2017

Keywords:
2-Phenylcyclopropane-1-carboxamides
1,1'-biphenyl-4-carboxamides
1,1'-biphenyl-2-carboxamides
G2/M arrest
Phospho-ATM and γH2AX increase

ABSTRACT

Several anthranilamide-based 2-phenylcyclopropane-1-carboxamides **13a-f**, 1,1'-biphenyl-4-carboxamides **14a-f** and 1,1'-biphenyl-2-carboxamides **17a-f** were obtained by a multistep procedure starting from the (1S,2S)-2-phenylcyclopropane-1-carbonyl chloride **11**, the 1,1'-biphenyl-4-carbonyl chloride **12** or the 1,1'-biphenyl-2-carbonyl chloride **16** with the appropriate anthranilamide derivative **10a-f**. Derivatives **13a-f**, **14a-f** and **17a-f** showed antiproliferative activity against human leukemia K562 cells. Among these derivatives **13b**, **14b** and **17b** exerted a particular cytotoxic effect on tumor cells. Derivative **17b** showed a better antitumoral effect on K562 cells than **13b** and **14b**. Analyses performed to explore **17b** mode of action revealed that it induced an arrest in G2/M phase of cell cycle which was consequent to DNA lesions as demonstrated by the increase in phospho-ATM and γH2AX, two known markers of DNA repair response system. The effect of **17b** was also related to ROS generation, activation of JNK and induction of caspase-3 dependent apoptosis.

1. Introduction

Our research group has long been interested in the chemistry and pharmacology of small molecules aiming to study their biological activity [1–10].

In particular, while a screening program was being carried out in order to find antiproliferative compounds in our laboratory's collection of small organic molecules, it has been found that the 2-cinnamamido-5-iodobenzamide **1** (Fig. 1) has an IC_{50} of 0.57 μM. This evidence considered, compound **1** was used as model to investigate extensively the antiproliferative activity of 2-cinnamamido, 2-(3-phenylpropiolamido) and 2-(2-phenoxyacetamido)benzamides [11–13]. Among these, compounds **1**–**6** (Fig. 1) resulted being the most active of the series. Taking into account the benzamide analogues reported previously, the data gathered showed the positive effects following substitution at the 5 position of the benzamido moiety, especially when the substituent(s) was iodine or 4,5-dimethoxy. Moreover, the simultaneous introduction of a substituent into both the benzamido and cinnamamido or phenylpropiolamido or phenoxyacetamido moieties is unfavorable for inhibition of K562 cell growth, despite the maintenance of antiproliferative activity in some ortho derivatives (Fig. 1, compounds **2**). The substitution of vinylene and ethynylene groups (Fig. 1, compounds **1**–**4**) with the methylenoxy moiety (Fig. 1, compounds **5**–**6**) was particularly interesting.

This chemical alteration affected the mode of action of derivatives. In fact, the mechanism of action is influenced by the scaffold bound to the benzamido skeleton. There is a G2/M arrest of cell cycle when the benzamido skeleton brings the cinnamamido or 3-phenylpropiolamido scaffold [11,12], but a cell block occurs in G0/G1 with activation, after 48 h, of caspase 3 and 6, whether the phenoxyacetamido scaffold is present.

* Corresponding author.
** Corresponding author.
E-mail addresses: demraffa@unipa.it (D. Raffa), benedetta.maggio@unipa.it (B. Maggio).

http://dx.doi.org/10.1016/j.ejmech.2017.03.051
0223-5234/

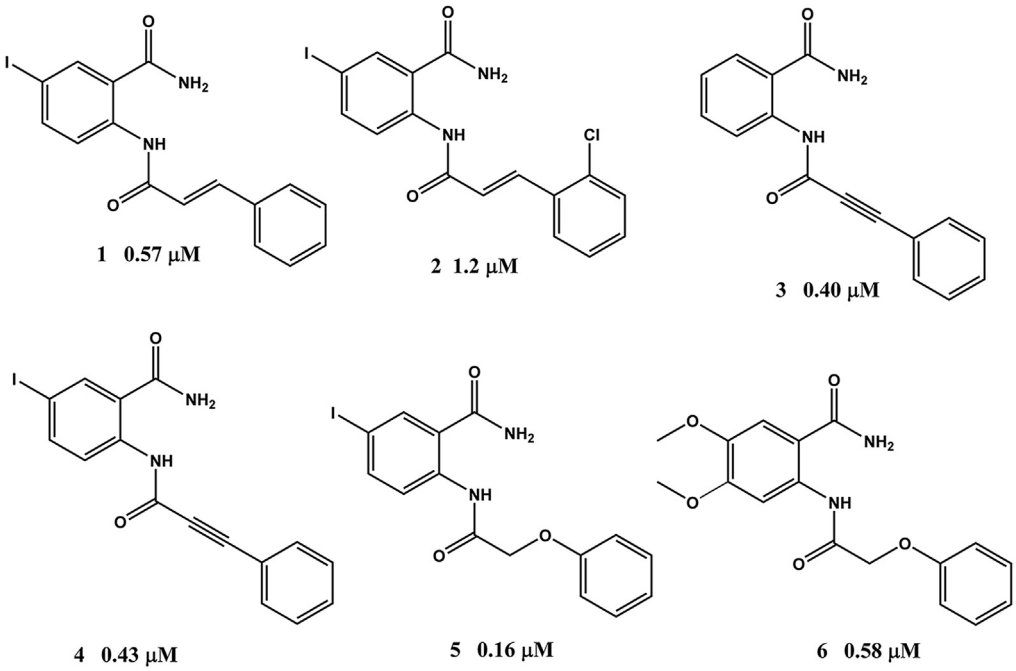

Fig. 1. The most active compounds among the previously synthesized benzamides [11–13].

Therefore, this paper is intended for a valuable clarification of the relationship between the mechanism of action and the scaffold bound to the benzamido skeleton by synthesizing new benzamido derivatives bearing the (1S,2S)-2-phenyl-cyclopropane-1-carboxamido, 1,1'-biphen-2-carboxamido and 1,1'-biphen-4-carboxamido moieties (Fig. 2, compounds **7**–**9**).

2. Results and discussion

2.1. Chemistry

The synthesis of the benzamido derivatives **13a-f** and **14a-f** were obtained, as reported in Scheme 1, by placing in an ice bath and under magnetic stirrer a mixture of the (1S,2S)-2-phenylcyclopropane-1-carbonyl chloride **11** or the 1,1'-biphenyl-4-carbonyl chloride **12** with the appropriate 5-R-4- R1-2-amminobenzamide **10a-f**. The (1S,2S)-2-phenylcyclopropane-1-carbonyl chloride **11** and the 1,1'-biphenyl-4-carbonyl chloride **12** were obtained refluxing the corresponding acids with thionyl chloride [14].

The attempt to obtain the 1,1'-biphenyl-2-carbonyl chloride **16** with the same method failed, yielding the 9H-fluoren-9-one **15** (Scheme 2).

Chloride **16** was obtained under milder conditions [15] by reacting at room temperature the 1,1'-biphenyl-2-carboxylic acid **14** with thionyl chloride in anhydrous chloroform and pyridine. The reaction and all the subsequent handling, including the distillation under vacuum of the reaction solvent, must have been conducted at room temperature since the temperature increases invariably cause the transformation to fluorenone **15**. Ultimately, the benzamido derivatives **17a-f** were obtained, as reported in Scheme 2, by placing in an ice bath and under magnetic stirrer a mixture of the 1,1'-biphenyl-2-carbonyl chloride **16** with the appropriate 5-R-4-R1-2-amminobenzamide **10a-f**. The anthranilamide **10a** is commercially available, whilst the 5-R-4-R1-2-aminobenzamides **10b-f** were obtained according to Scheme 3. In specific terms, the 5-iodo-2-aminobenzamide **10b** was obtained, as reported in the literature [16], by treatment of anthranilamide **10a** with iodine in an aqueous solution of sodium bicarbonate. The anthranilamides **10c-f** were obtained by reduction of 2-nitro-5-methyl benzamides **20c-f** as displayed in Scheme 3. Compounds **20c-f** were obtained by reaction of the acids **18c-f** with thionyl chloride to afford **19c-f**, followed by treatment of **19a-c** with aqueous ammonia.

The structures of the new compounds were determined by analytical and spectroscopic measurements. Going into details, **13a-f**, **14a-f** and **17a-f** showed 1H NMR signals attributable to aromatic protons in the range 7.01–8.77 δ and a singlet in the range 13.05–11.51 δ, exchangeable with D_2O, for the amidic NH. For the signals of the NH_2 benzamido protons, as previously reported for the 2-(2-phenoxyacetamido) benzamides [13], the presence of an intramolecular hydrogen bond rendered the benzamido NH_2 protons diastereotopic. Ha appeared as a singlet along with aromatic multiplets whereas Hb was found at a lower field as a singlet at 8.06–8.56 δ.

Furthermore, derivatives **13a-f** showed the characteristic signals of the trans 1,2-cyclopropane system at about 2.43 and 1.94 δ attributable to the two CH, and at 1.52 and 1.39 δ for the two hydrogens of the methylene. Conclusively, the 1H-NMR spectra of methyl and methoxy-substituted derivatives **13d-f**, **14d-f** and **17d-f** showed signals in the range 3.33–3.87 δ and at about 2.29 δ arising from the methoxyl and methyl groups respectively.

2.2. Biology

Synthesized benzamido derivatives **13a-f**, **14a-f** and **17a-f** were preliminarily tested in vitro for their antileukemic activity against the K562 cells, a human chronic myelogenous leukemia cell line; colchicine, whose antileukemic activity is renowned, was used as reference compound. The percent growth inhibition at a screening concentration of 10 μM is shown in Table 1. The tested compounds had inhibitory activity against the K562 cells ranging from 15.0 to 85.0% at 10 μM (24 h), with **17b** (85.0%), being the most active compound. By analogy with the previously reported benzamide analogues [11–13], the antitumor efficacy of compound **17b** is

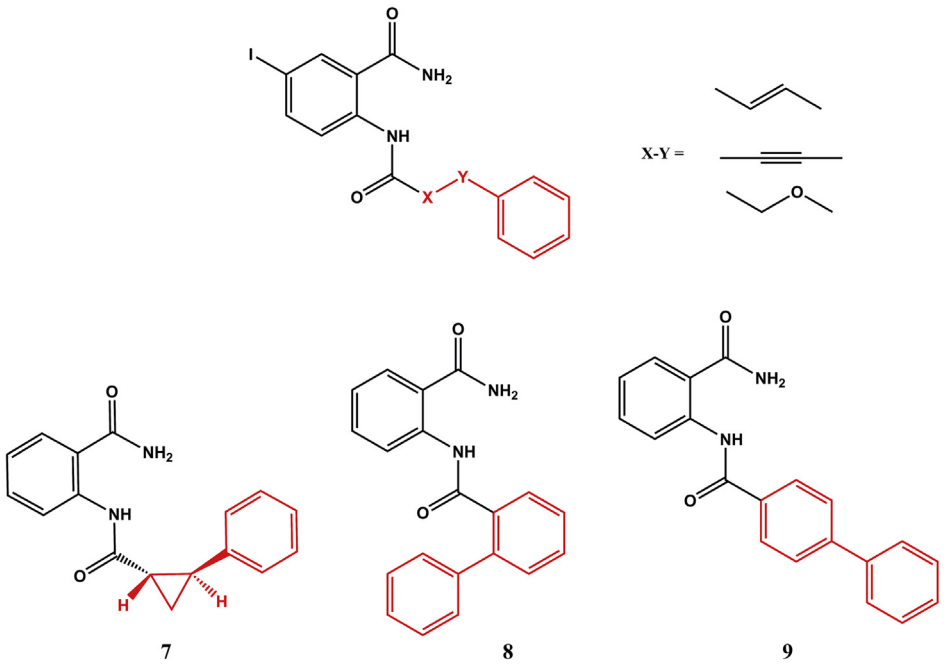

Fig. 2. Structural modifications on the scaffold bound to the benzamido skeleton.

related to the substitution at the 5 position of the benzamido moiety, eminently with iodine.

The antitumor activity of **17b** was also investigated, germane to other two cancer cell lines: human colon cancer HT29 cells and human triple-negative breast cancer MDA-MB231 cells. As shown in Table 2, **17b** exerts antitumor effects in both the tumor cell lines, although they were visible at higher doses than those used in K562 cells, as a result K562 is the most sensitive cell line to **17b**. In addition, the activity of **17b** was also evaluated on 16HBE, a human normal bronchial epithelial cell lines. Interestingly, the effect of **17b** was less pronounced than in K562 cells (16HBE/K562 index 60), thus suggesting that this compound exerts reduced toxicity in normal cells (Table 2).

Compound **17b**, bearing the 2-1,1'-biphenyl moiety, was also selected for further biological studies. Derivatives **13b** and **14b**, representative of the other two classes of derivatives (2-((1R,2R)-2-phenylcyclopropane-1-carboxamido)benzamides and N-(2-carbamoylphenyl)-[1,1'-biphenyl]-4-carboxamides) were also taken into account because they have the same substituent of **17b** in the 5 position (iodine). Firstly, the antiproliferative activity of

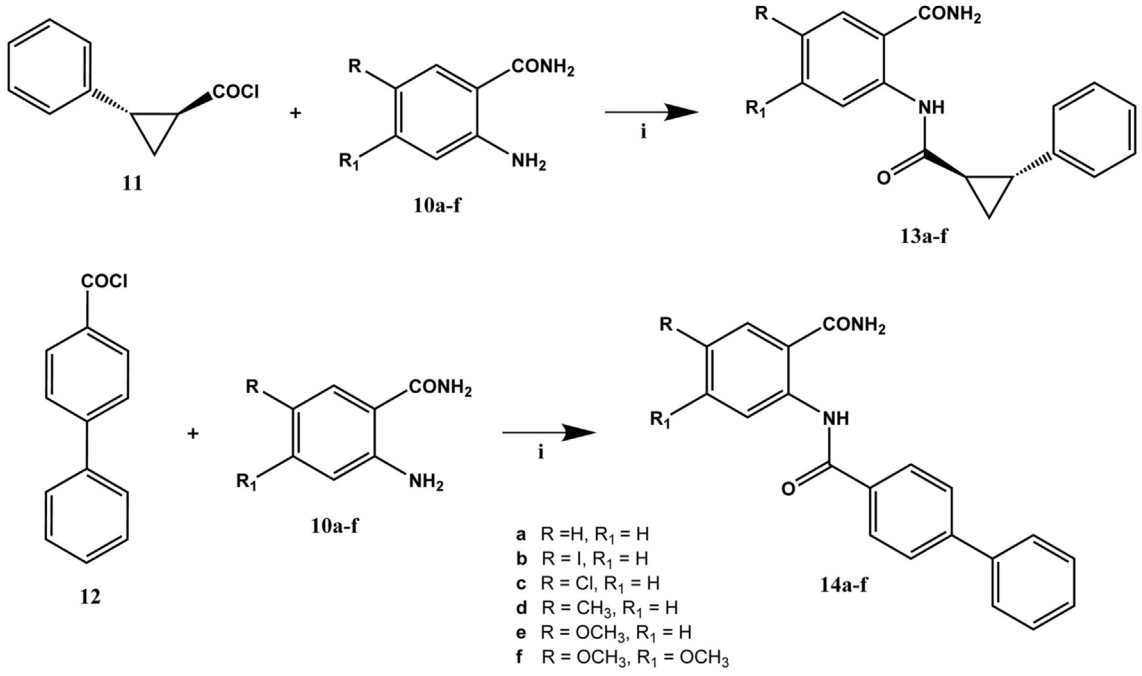

Scheme 1. Synthetic pathway for the formation of benzamido derivatives **13a-f** and **14a-f**: **i** T = 0–5°, pyridine.

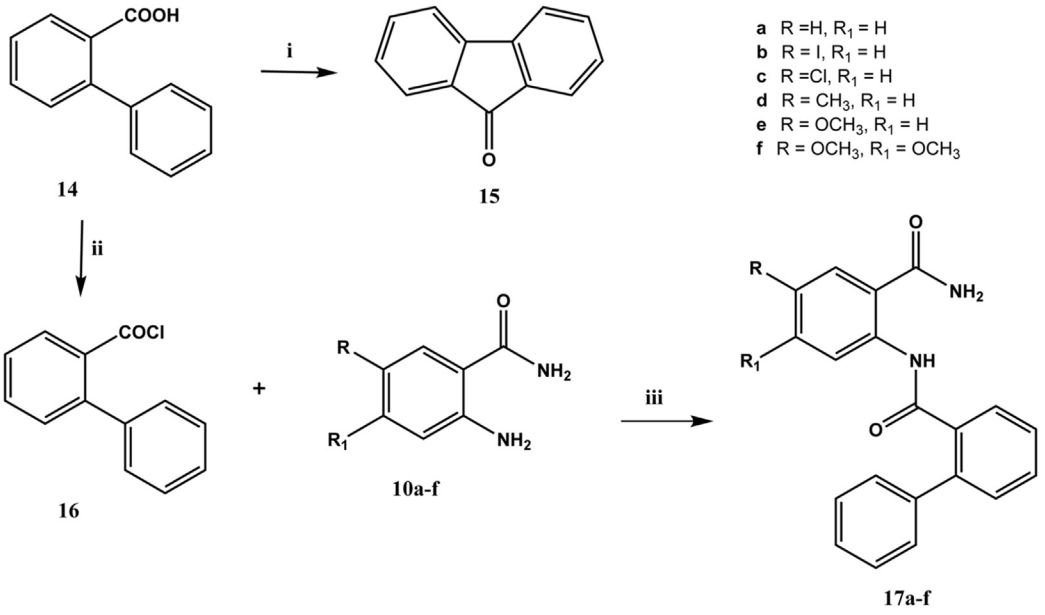

Scheme 2. Synthetic pathway for the formation of benzamido derivatives **17a-f**: **i** reflux, thionyl chloride; **ii** $CHCl_3$/pyridine, thionyl chloride, room temperature; **iii** T = 0–5°, pyridine.

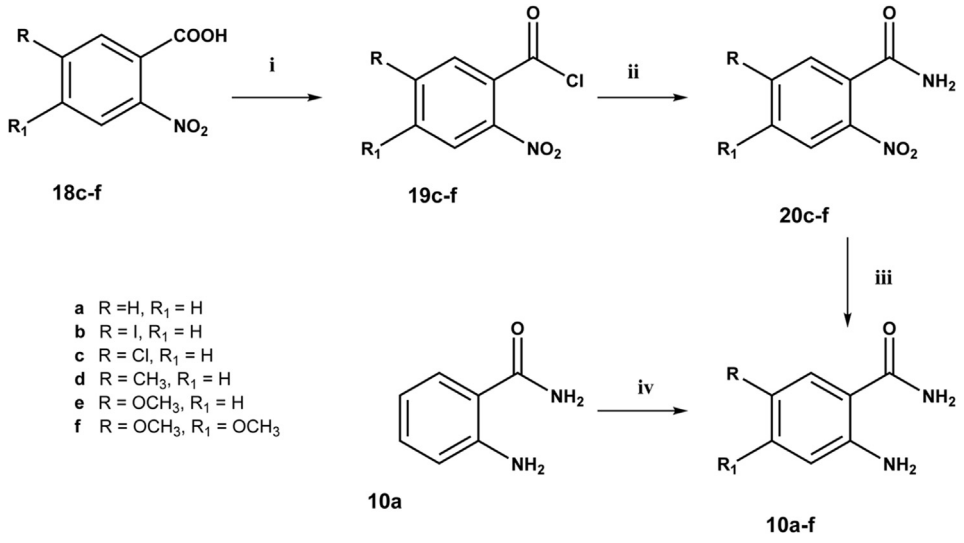

Scheme 3. Synthetic pathway for the formation of derivatives **10a-f**: **i** thionyl chloride $CHCl_3$/pyridine; **ii** ammonia; **iii** $SnCl_2$/HCl 37%; **iv** I_2, aqueous sodium bicarbonate.

Table 1
Percent growth inhibition obtained with the K562 cell line with compounds at 10 μM at 24 h.

Comp.	K562 (10 μM)	Comp.	K562 (10 μM)
13a	ns	**14e**	29.2
13b	25.0	**14f**	48.0
13c	24.0	**17a**	44.6
13d	15.0	**17b**	85.0
13e	26.7	**17c**	47.3
13f	26.7	**17d**	48.9
14a	21.6	**17e**	37.0
14b	15.0	**17f**	46.0
14c	45.0	**COL**	63.6
14d	39.7		

ns not significant (% inhibition <10%). COL = Colchicine.

compounds **13b**, **14b** and **17b** was explored towards K562 by means of different concentrations of each compound (within the range of 500 nM-25 μM) for up to 48 h and evaluating the cell viability by a MTT assay, as reported in Methods. All the three compounds reduced the viability of K562 cells in a dose-and time-dependent manner with IC_{50} values at 48 h, ranging from 500 nM to 15 μM (Fig. 3A).

Table 2
Comparison of IC_{50} values (μM) between 16HBE cells and K562, HT26 and MDA-MB231 cells.

Cell lines	IC_{50}	Cell line/16HBE
K562	0.5	60
HT26	10	3
MDA-MB231	10	3
16HBE	30	

Values are the mean of at least three independent determination.

Interestingly, **17b** showed a greater antiproliferative activity against K562 cells (IC_{50} 0.5 μM at 48 h) than **13b** and **14b** compounds (at 48 h IC_{50} was 10 and 15 μM, respectively) (Fig. 3A). Morphological analyses of K562 cells, performed by a phase contrast microscope, showed that all analyzed compounds exerted a clear cytotoxic effect which resulted more pronounced in **17b**-treated cells.

As Fig. 3B shows, the exposure to **17b** induced a cell number and volume reduction with the appearance of shrunken cytoplasm at 24 h, followed by a widespread cell fragmentation at 48 h. Successively, comparative experiments were carried out to examine the effects of compounds **13b**, **14b** and **17b** on the distribution of cells in the different phases of cell cycle. To this purpose, the DNA content along cell cycle phases was determined by a flow cytometric assay after staining of the cells with propidium iodide (PI), a fluorescent dye which intercalates into the major groove of double-stranded DNA. As evident in Fig. 4A, treatment with **17b** resulted at 24 h in a significant increase in the proportion of K562 cells in G2/M phase compared to untreated control cells.

In response to DNA damage, members of phosphoinositide 3-kinase related to protein kinases (PIKKs), such as ATM (ataxia-telangiectasia mutated) and ATR (ATM and RAD3-related) kinases, were recruited at the chromatin lesions and in turn activated by phosphorylation [17]. These kinases, once activated, promote the phosphorylation of key factors which regulate the cell cycle arrest, the DNA repair and the apoptosis induction [18]. ATR is mainly activated by both a structure containing single-stranded DNA (ssDNA) and ssDNA and double-stranded DNA (dsDNA) junction, whereas ATM activation is promoted in response to double-strand breaks (DSBs) [18]. By using a specific antibody, directed against the phosphorylated Ser1981 of ATM, it has been discovered that the treatment with **17b** caused in K562 cells a marked phosphorylation of ATM at this residue. This effect, which resulted particularly pronounced after 24 h of treatment but decreased at 48 h (Fig. 5A). In response to DNA DSBs, ATM phosphorylates histone H2AX at Ser139 residue to form γH2AX [19].

The importance of this post-translational modification relies on the ability of γH2AX to mark the damaged DNA, facilitating local recruitment and retention of DNA repair and chromatin remodeling factors to restore genomic integrity [19]. It was conjointly

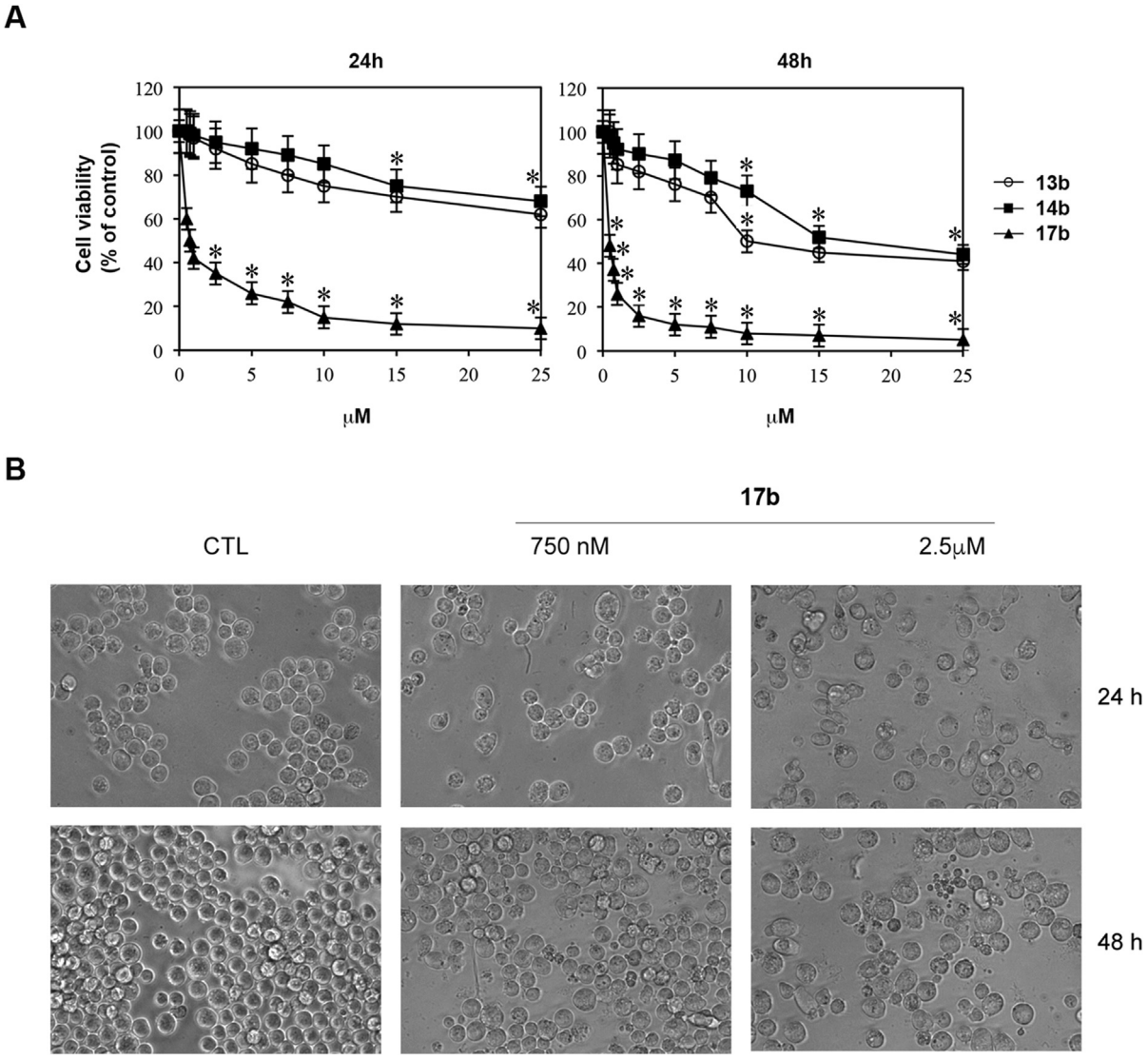

Fig. 3. Antiproliferative effects of **13b**, **14b** and **17b** on K562 cells. Cells (8×10^3/well) were treated with different doses of the three compounds (**13b**, **14b** and **17b**) for 24 and 48 h, respectively. In A cell viability was assessed by MTT assay as reported in method section. In B micrographs of morphological features of cells treated with **17b** and observed under a light microscope using Leica IM50 software are reported. Original magnification was 200×. *$p < 0.05$ vs control.

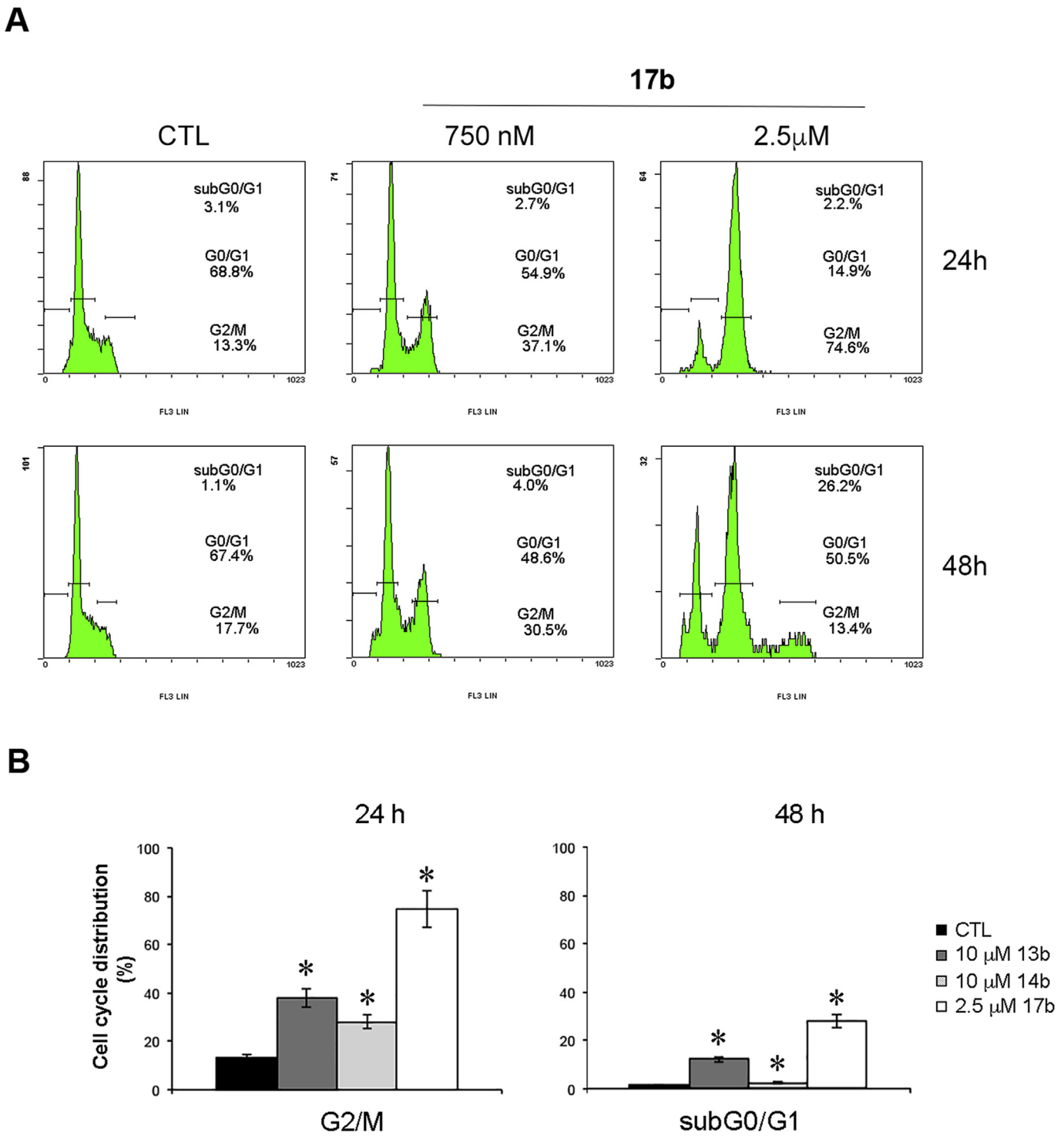

Fig. 4. Cell cycle distribution of K562 cells after exposure to **13b**, **14b** or **17b** compound. (A) Cytofluorimetric histogram data representing the effect of **17b** compound. (B) Comparative analysis of G2/M and subG0/G1 cell population in K562 cells incubated in the absence or in the presence of **13b, 14b or 17b** compound. In (A) and (B) cells (1.5×10^5) were incubated for the indicated times with the compounds. Then, cells were harvested, stained with propidium iodide (PI) as described in Methods section and the amount of PI-positive cells was quantified by flow cytometry. In (A) x-axis indicates fluorescence intensity on linear scale and y-axis the number of events. Percentages of cells in the subG0/G1 region which reports the amount of fragmented DNA was considered as an index of apoptosis. At least 10,000 events per sample were measured. *$p < 0.05$ vs control.

demonstrated that **17b** markedly increased in K562 cells the level of phosphorylated H2AX at the Ser139 in a dose-and time-dependent manner (Fig. 5A). All things considered, these findings suggest that **17b** causes DNA double-strand breaks (DSBs) leading to ATM activation followed by Ser139 phosphorylation of H2AX (γH2AX). It is additionally noteworthy that after DNA damage the cells undergo apoptosis if the repair mechanisms fail [17]. In the analyses conducted, cytofluorimetric assays showed that **17b** increased the percentage of cells in subG0/G1 phase, indicative of cells with fragmented DNA. On that account, a further analysis was carried out in order to verify whether **17b** was able to induce apoptosis, by Hoechst 33342 staining. Representative pictures of **17b** effects on of

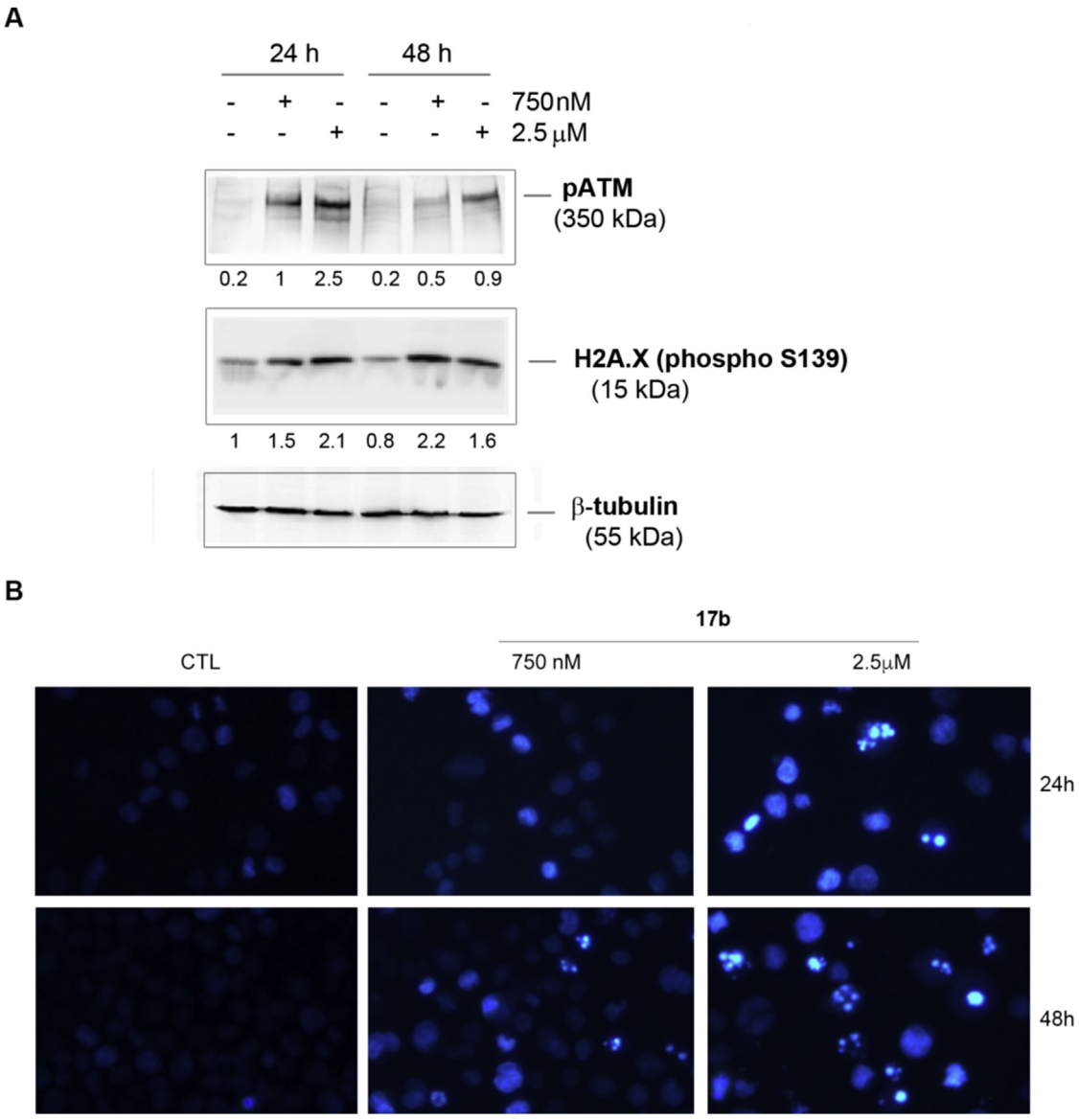

Fig. 5. Analysis of DNA damage in K562 cells treated with **17b** compound. (A) Effect of **17b** compound on phospho-ATM and γH2AX protein expression level. K562 cells (1.5×10^5/well) were treated for 24 and 48 h with 750 nM and 2.5 μM doses, then cell extracts were prepared and, following gel electrophoresis, subjected to Western blotting analysis to determine the levels of proteins. The fold changes were calculated normalizing to housekeeping β-tubulin protein (loading control). Results are representative of three independent experiments. (B) Fluorescence micrographs showing the effects of **17b** compound on K562 cells after Hoechst 33342 staining. K562 cells (8×10^3/well) were stained with Hoechst 33342 (2.5 μg/ml medium; blue fluorescence) and then treated with 750 nM and 2.5 μM **17b** for 24 and 48 h. Cell morphology was visualized with a Leica DC 300F microscope with a fluorescence filter for DAPI. Original magnification was 200×. The images acquired using Leica Q Fluoro show details of cells with clear signs of apoptosis, such as nuclear shrinkage, chromatin condensation and DNA fragmentation. (For interpretation of the references to colour in this figure legend, the reader is referred to the web version of this article.)

K562 cells are reported in Fig. 5B, demonstrating the activation of apoptosis by **17b**. As a matter of fact, notwithstanding that in control cells nuclei appeared rounded and homogeneously stained, after treatment with **17b** the cells displayed characteristic signs of apoptosis such as cell shrinkage, chromatin condensation and fragmentation (Fig. 5B). Cells with fragmented DNA appeared already after 24 h of treatment with **17b** and their number markedly increased after 48 h, in accordance with the cytofluorimetric analyses.

Consequently, to evaluate whether **17b**-induced apoptosis was due to the activation of caspases, the ability of **17b** to activate caspase-3 in K562 cells was analyzed. Caspase-3 is an effector caspase in the last and irreversible phase of the apoptotic caspase-dependent pathway, which is activated by the cleavage of a pro-caspase inactive form [13].

The level of procaspase-3 was detected by western blotting analyses in K562 cells treated with **17b** for 24 or 48 h. Fig. 6B shows a decrease in the level of procaspase-3, indicative of caspase-3 activation, in K562 cells treated with both 750 nM and 2.5 μM **17b**. The effect, which was already visible after 24 h of treatment, further increased at 48 h, in accordance with the pronounced DNA fragmentation observed by Hoechst stained cells. Many experimental evidences supported the link between the DNA damage response (DDR) cascade and reactive oxygen species (ROS) signaling, reporting these processes as key events in the induction of cell death after DNA damage. In particular, it has been demonstrated that DNA damage can significantly increase ROS intracellular level through histone H2AX, Nox1, and Rac1 [20]. Differently,

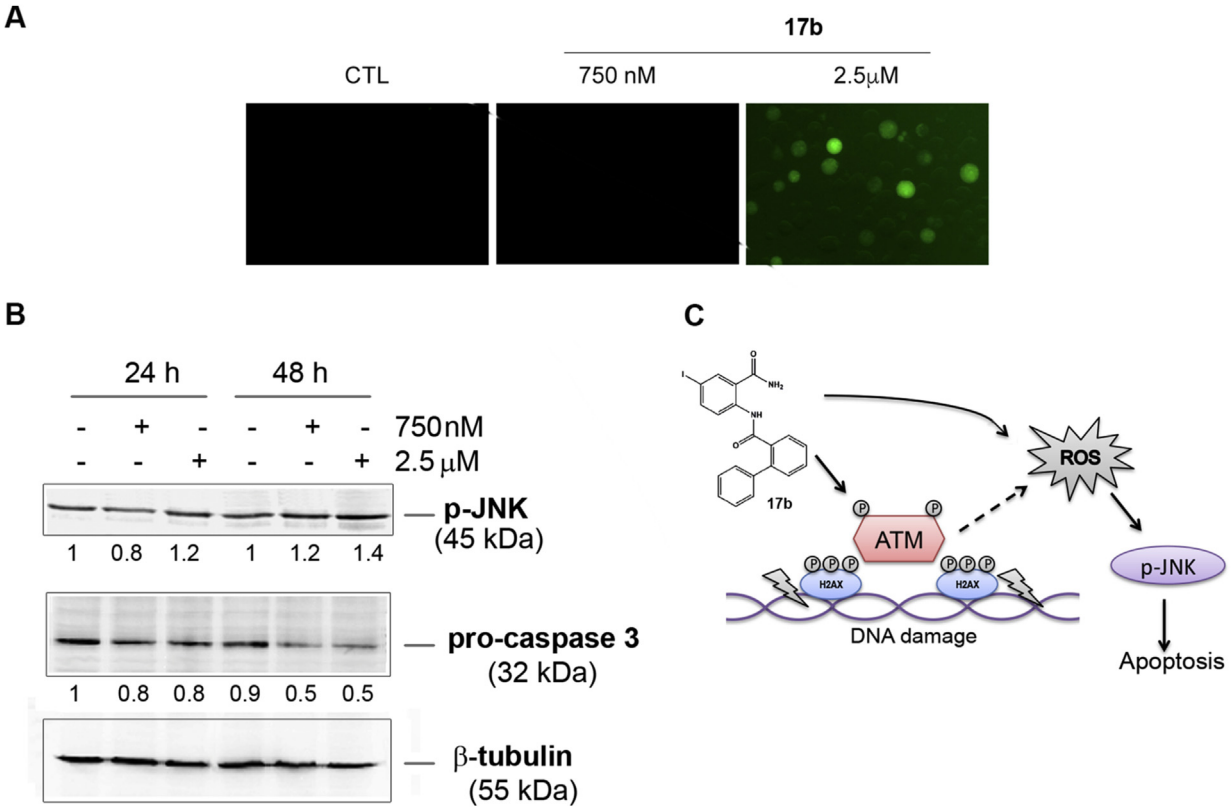

Fig. 6. Analysis of reactive oxygen species generation, phospho-JNK and caspase-3 activation induced by **17b** compound treatment. (A) Fluorescence microscopy images showing reactive oxygen species (ROS) production by **17b** treatment for 48 h. Original magnification was 200×. (B) Western blot of phospho-JNK and the apoptotic marker caspase-3 in K562 cells treated with **17b**. K562 cells (1.5×10^5/well) were treated for 24 and 48 h with 750 nM and 2.5 μM **17b**. Cell extracts were prepared and, following gel electrophoresis, subjected to Western blotting analysis to determine the levels of pro-caspases 3. The fold changes were calculated normalizing to housekeeping β-tubulin protein (loading control). Results are representative of three independent experiments. (C) Schematic representation of the mode of action of **17b** compound in K562 cells. **17b** compound induces DNA damage, increases γH2AX and phospho-ATM after 24 h. Prolonged treatment (48 h) with **17b** causes ROS production, activation of phospho-JNK and consequently induction of apoptotic cell death.

compelling evidences have indicated besides ROS as effectors of DNA breaks in some cell systems [21]. Provided the interest in establishing whether the **17b**-induced DNA damage could be associated to ROS generation and elucidating the causative relationship of these two events, the H2DCFDA-based assay was used. H2DCFDA is a dye that passively diffuses through cell membrane and, inside the cell, loses its acetate groups by an intracellular esterase-mediated cleavage. In the presence of pro-oxidants it yields a green fluorescent adduct that is entrapped inside the cell, therefore the distinction of cells producing ROS as green stained cells under a fluorescence microscope is plainly possible.

Hence, time course experiments were performed after the exposure of the cells to the drug for 5, 24 and 48 h, respectively. The data elaborated provide evidence that ROS production was not observed for brief times of incubation (5–24 h, data not shown), while its generation appeared after 48 h of treatment (Fig. 6A). In fact, K562 cells exposed for 48 h to **17b** treatment appeared stained in green in comparison with the untreated control cells. Thus, this result suggests that oxidative stress, which was visible only at 48 h of treatment, cannot be considered as a causative event in **17b**-induced DNA damage, but it can be responsible of the induction of apoptosis in accordance with other authors' observations [22].

As a consequence of ROS generation, our studies also testified that **17b** increased in K562 cells the level of the phosphorylated and active form of c-Jun N-terminal kinase (JNK), a member of the superfamily of mitogen-activated protein kinase (MAPK), which can be induced by ROS production [23] and promote caspase-dependent cell death [24]. As Fig. 6B shows, the phosphorylation of JNK appeared after 24 h of treatment with **17b** and further increased at 48 h.

3. Conclusion

The data reported in this study show that the benzamido derivatives **13**, **14** and **17** exerted an antiproliferative action on K562, a human chronic myelogenous leukemia cell line. The best effects were observed with **13b**, **14b** and **17b** derivatives which showed an IC_{50} at 48 h with 10, 15 and 0.5 μM, respectively.

17b exerted cytotoxic effects in K562 leukemic cells at nanomolar concentrations, thus it was selected as compound to explore its mode of action. In specific terms, the data provide evidence that this compound induced double-strand DNA damage, as shown by accumulation of histone γH2AX. DNA damage in turn led to cell cycle arrest in G2/M phase followed by induction of a caspase-dependent apoptosis after prolonged treatment. These effects were accompanied by ROS production, JNK phosphorylation and induction of apoptosis. ROS production could be induced by DNA damage, in line with the observation of Kang et al. [14]. Alternatively, it could result by an altered balance between pro-oxidant and anti-oxidant systems. A possible schematic model of **17b**-induced cytotoxic effects in K562 cells is reported in Fig. 6C.

Conclusively, this work highlights the different behavior of benzamido derivatives **13a-f**, **14a-f** and **17a-f** bearing the (1S,2S)-2-phenyl-cyclopropane-1-carboxamido, 1,1'-biphen-2-carboxamido and 1,1'-biphen-4-carboxamido scaffolds (G2/M arrest of cell cycle and DNA lesions with increase in phospho-ATM and γH2AX), in

comparison with cinnamamido and 3-phenylpropiolamido benzamides (G2/M arrest of cell cycle and antitubulinic activity) [11,12] previously studied, as well as phenoxyacetamido benzamides (G0/G1 arrest of cell cycle) [13].

4. Experimental

4.1. Chemistry

4.1.1. General

Reaction progress was monitored by TLC on silica gel plates (Merck 60, F_{254}, 0.2 mm). Organic solutions were dried over Na_2SO_4. Evaporation refers to the removal of solvent on a rotary evaporator under reduced pressure. All melting points were determined on a Büchi 530 capillary melting point apparatus and are uncorrected. IR spectra were recorded with a Perkin Elmer Spectrum RXI FT-IR System spectrophotometer, with compound as a solid in a KBr disc or nujol. ^{1}H NMR (300 MHz) and APT (75 MHz) spectra were recorded with a Bruker AC-E spectrometer at r.t.; chemical shifts (δ) are expressed as ppm values. Microanalyses data (C, H, N) were obtained by an Elemental Vario EL III apparatus and were within ±0.4% of the theoretical values. Yields refer to purified products and are not optimized. The names of the compounds were obtained using Chem Draw Ultra 12.0 software (CambridgeSoft).

4.1.2. General procedure for preparation of 5-R-4-R_1-2-nitrobenzoyl chlorides ***19c-f***, the (1S,2S)-2-phenylcyclopropane-1-carbonyl chloride ***11*** and the 1,1'-biphenyl-4-carbonyl chloride ***16*** [14].

The 5-R-4-R_1-2-nitrobenzoyl chlorides **19c-f**, the (1S,2S)-2-phenylcyclopropane-1-carbonyl chloride **11** and the 1,1'-biphenyl-4-carbonyl chloride **16** were obtained by refluxing for 5 h the appropriate acid derivatives (0.01 mol) with thionyl chloride (7.25 mL). After evaporation under reduced pressure, the crude liquid residue was used for subsequent reactions without purification.

4.1.3. Preparation of 1,1'-biphenyl-2-carbonyl chloride ***12***

The 1,1'-biphenyl-2-carbonyl chloride **12** was obtained by reacting 1,1'-biphenyl-2-carboxylic acid **14** with thionyl chloride according to the procedure reported by Babalan [15]. The crude liquid residue was used for subsequent reactions without purification.

4.1.4. Preparation of 5-R-4-R_1-2-nitrobenzamides ***20c-f*** [13]

To 10 mmol of 5-R-4-R_1-2-nitrobenzoyl chlorides **19c-f** 10 mL of an aqueous ammonia solution (25%) and 33 mL of acetonitrile were added. The solution was first refluxed for 8 h, and then evaporated to give pure **20c-f**.

4.1.5. Preparation of 5-R-4-R_1-2-aminobenzamides ***10c-f*** [13]

To a magnetically stirred suspension of stannous chloride (38 mmol) in concentrated HCl (37%), 13 mmol of **20c-f** was added (15 mL) at a rate so that the temperature of the slurry was maintained below 5 °C (about 1 h). After addition was complete, the mixture was stirred for 24 h. The white slurry thus obtained was diluted with cold water (150 mL), and NaOH (40%) was added until the tin salt dissolved. The solution was extracted with ethyl acetate (3 × 150 mL), and the extracts dried and evaporated to obtain pure **10c-f**.

4.1.6. General procedure for preparation of 2-amino-5-iodobenzamide ***10b*** [16]

Powdered iodine (11.7 g, 46.2 mmol) was added portion-wise over 1 h to a stirred solution of 2-aminobenzamide **10a** (5.72, 42.0 mmol) and $NaHCO_3$ (3.52 g, 42.0 mmol) in water (1.3 l). The solution was stirred overnight at room temperature. Afterwards $NaHSO_3$ (0.87 g, 8.40 mmol) was added. The solution was extracted with ethyl acetate (3 × 800 ml). After being dried with Na_2SO_4, the organic phase was removed under reduced pressure. The crude product was recrystallized with water/methanol 10:1 v/v, 600 ml) to yield pure **10b**; yield 95%, mp 197–198 °C.

4.1.7. General procedure for preparation of 5-R-4-R_1-2-((1S,2S)-2-phenylcyclopropane-1-carboxamido)benzamides ***13a-f***, N-(2-carbamoyl-4-R-5-R_1-phenyl)-[1,1'-biphenyl]-4-carboxamide ***14a-f*** and N-(2-carbamoyl-4-R-5R_1-phenyl)-[1,1'-biphenyl]-2-carboxamide ***17a-f***

To a cold (0–5 °C) stirred suspension of aminobenzamides **10a-f** (16 mmol) in pyridine (13 mL), 16 mmol of the (1S,2S)-2-phenylcyclopropane-1-carbonyl chloride **11**, the 1,1'-biphenyl-4-carbonyl chloride **12** or the 1,1'-biphenyl-2-carbonyl chloride **16** chloride was added over 30 min. After addition was complete, the solution was stirred for 24 h and then poured onto crushed ice. The precipitate was removed by filtration, washed with water, and crystallized from the indicated solvent.

4.1.7.1. 2-((1R,2R)-2-phenylcyclopropane-1-carboxamido)benzamide (13a). 19% yield; mp 188–191 °C (ethanol); I.R. (KBr) cm^{-1} 3354, 3281, 3189 (NH, NH_2), 1675, 1656 (2 CO) ^{1}H-NMR (DMSO) δ 1.35–1.42 (m, 1H, cyclopropane CH-H); 1.50–1.56 (m, 1H, cyclopropane CH-H); 1.92–1.98 (m, 1H, cyclopropane CH); 2.40–2.47 (m, 1H, cyclopropane CH); 7.10–8.46 (set of signals, 11H, aromatic protons and exchangeable NH_2); 11.91 (s, 1H, NH; exchangeable with D_2O). ^{13}C-NMR (δ) (DMSO) 16.80, 25.67, 28.28, 120.10, 120.77, 122.83, 126.41, 126.62, 128.82, 129.02, 132.61, 139.95, 140.97, 170.19, 171.18. Anal. Calc. for $C_{17}H_{16}N_2O_2$: C, 72.84%; H, 5.75%; N, 9.99%. Found: C, 73.19%; H, 6.10%; N, 9,84%.

*4.1.7.2. 5-Iodo-2-((1R,2R)-2-phenylcyclopropane-1-carboxamido) benzamide (**13b**).* 53% yield; mp 200–205 °C (ethanol); I.R. (KBr) cm^{-1} 3296, 3189 (NH, NH_2), 1675, 1652 (2 CO) ^{1}H-NMR (DMSO) δ 1.35–1.41 (m, 1H, cyclopropane CH-H); 1.48–1.54 (m, 1H, cyclopropane CH-H); 1.93–1.99 (m, 1H, cyclopropane CH); 2.39–2.46 (m, 1H, cyclopropane CH); 7.19–8.36 (set of signals, 10H, aromatic protons and exchangeable NH_2); 11.81 (s, 1H, NH; exchangeable with D_2O). ^{13}C-NMR (δ) (DMSO) 16.90, 25.82, 28.19, 86.46, 122.46, 122.98, 126.45, 126.66, 128.82, 137.07, 139.49, 140.88, 140.93, 169.70, 170.34. Anal. Calc. for $C_{17}H_{15}IN_2O_2$: C, 50.26%; H, 3.72%; N, 6.90%. Found: C, 50.45%; H, 3.67%; N, 6,83%.

*4.1.7.3. 5-Chloro-2-((1R,2R)-2-phenylcyclopropane-1-carboxamido) benzamide (**13c**).* 15% yield; mp 320–324 °C (ethanol); I.R. (KBr) cm^{-1} 3353, 3293, 3189 (NH, NH_2), 1675, 1654 (2 CO) ^{1}H-NMR (DMSO) δ 1.36–1.42 (m, 1H, cyclopropane CH-H); 1.50–1.56 (m, 1H, cyclopropane CH-H); 1.95–2.00 (m, 1H, cyclopropane CH); 2.40–2.47 (m, 1H, cyclopropane CH); 7.19–8.47 (set of signals, 10H, aromatic protons and exchangeable NH_2); 11.77 (s, 1H, NH; exchangeable with D_2O). ^{13}C-NMR (δ) (DMSO) 16.91, 25.82, 28.12, 121.99, 122.61, 126.43, 126.63, 126.66, 128.62, 128.82, 132.23, 138.66, 140.87, 169.75, 170.36. Anal. Calc. for $C_{17}H_{15}ClN_2O_2$: C, 64.87%; H, 4.80%; N, 8.90%. Found: C, 64.68%; H, 4,53%; N, 9.25%.

*4.1.7.4. 5-Methyl-2-((1R,2R)-2-phenylcyclopropane-1-carboxamido) benzamide (**13d**).* 14% yield; mp 176–179 °C (ethanol); I.R. (KBr) cm^{-1} 3354, 3290, 3196 (NH, NH_2), 1672, 1651 (2 CO) ^{1}H-NMR (DMSO) δ 1.33–1.39 (m, 1H, cyclopropane CH-H); 1.48–1.54 (m, 1H, cyclopropane CH-H); 1.90–1.96 (m, 1H, cyclopropane CH); 2.30 (s, 3H, CH_3); 2.38–2.44 (m, 1H, cyclopropane CH); 7.18–8.33 (set of signals, 10H, aromatic protons and exchangeable NH_2); 11.75 (s, 1H, NH; exchangeable with D_2O). ^{13}C-NMR (δ) (DMSO) 16.73, 20.79,

25.54, 28.22, 120.25, 120.79, 126.39, 126.59, 128.81, 129.30, 131.85, 133.01, 137.49, 141.03, 169.94, 171.20. Anal. Calc. for $C_{18}H_{18}N_2O_2$: C, 73.45%; H, 6.16%; N, 9.52%. Found: C, 73.70%; H, 6.21%; N, 9.15%.

*4.1.7.5. 5-Methoxy-2-((1R,2R)-2-phenylcyclopropane-1-carboxamido)benzamide (**13e**).* 13% yield; mp 197–200 °C (ethanol); I.R. (KBr) cm^{-1} 3361, 3305, 3179 (NH, NH_2), 1655, 1618 (2 CO) ^{1}H-NMR (DMSO) δ 1.35–1.37 (m, 1H, cyclopropane CH-H); 1.47–1.51 (m, 1H, cyclopropane CH-H); 1.91–1.94 (m, 1H, cyclopropane CH); 2.39–2.42 (m, 1H, cyclopropane CH); 3.33 (s, 3H, OCH_3); 7.06–8.33 (set of signals, 10H, aromatic protons and exchangeable NH_2); 11.52 (s, 1H, NH; exchangeable with D_2O). ^{13}C-NMR (δ) (DMSO) 16.08, 24.83, 27.48, 55.33, 113.16, 117.52, 121.15, 122.18, 125.84, 126.01, 128.25, 132.44, 140.55, 154.07, 169.18, 170.17. Anal. Calc. for $C_{18}H_{18}N_2O_3$: C, 69.66%; H, 5.85%; N, 9.03%. Found: C, 69.99%; H, 6.23%; N, 9.32%.

*4.1.7.6. 4,5-Dimethoxy-2-((1R,2R)-2-phenylcyclopropane-1-carboxamido)benzamide (**13f**).* 21% yield; mp 200–203 °C (ethanol); I.R. (KBr) cm^{-1} 3420, 3299, 3203 (NH, NH_2), 1659, 1641 (2 CO) ^{1}H-NMR (DMSO) δ 1.34–1.41 (m, 1H, cyclopropane CH-H); 1.51–1.55 (m, 1H, cyclopropane CH-H); 1.84–1.89 (m, 1H, cyclopropane CH); 2.38–2.46 (m, 1H, cyclopropane CH); 3.46 (s, 6H, 2 OCH_3); 7.18–8.29 (set of signals, 9H, aromatic protons and exchangeable NH_2); 12.36 (s, 1H, NH; exchangeable with D_2O). ^{13}C-NMR (δ) (DMSO) 16.59, 25.22, 28.53, 55.80, 56.35, 103.95, 110.46, 112.01, 126.40, 126.61, 128.82, 135.88, 141.00, 143.75, 151.93, 169.88, 171.04. Anal. Calc. for $C_{19}H_{20}N_2O_4$: C, 67.05%; H, 5.92%; N, 8.23%. Found: C, 67.07%; H, 6.19%; N, 7.88%.

*4.1.7.7. N-(2-carbamoylphenyl)-[1,1'-biphenyl]-4-carboxamide (**14a**).* 45% yield; mp 225–230 °C (ethanol); I.R. (KBr) cm^{-1} 3376, 3206, 3189 (NH, NH_2), 1654, 1633 (2 CO) ^{1}H-NMR (DMSO) δ 7.17–8.76 (set of signals, 15H, aromatic protons and exchangeable NH_2); 13.05 (s, 1H, NH; exchangeable with D_2O). ^{13}C-NMR (δ) (DMSO) 119.04, 104.16, 119.95, 122.55, 126.86, 127.05, 127.55, 128.16, 128.67, 128.98, 132.52, 133.27, 138.84, 140.06, 143.46, 163.96, 171.13. Anal. Calc. for $C_{20}H_{16}N_2O_2$: C, 75.93%; H, 5.10%; N, 8.86%. Found: C, 75.82%; H, 5.13%; N, 8.77%.

*4.1.7.8. N-(2-carbamoyl-4-iodophenyl)-[1,1'-biphenyl]-4-carboxamide (**14b**).* 46% yield; mp 250–255 °C (ethanol); I.R. (KBr) cm^{-1} 3384, 3273, 3210 (NH, NH_2), 1668, 1655 (2 CO) ^{1}H-NMR (DMSO) δ 7.44–8.56 (set of signals, 14H, aromatic protons and exchangeable NH_2); 12.95 (s, 1H, NH; exchangeable with D_2O). ^{13}C-NMR (δ) (DMSO) 86.27, 121.18, 122.21, 126.93, 127.14, 127.64, 128.26, 129.05, 133.07, 136.77, 138.85, 139.74, 140.94, 143.65, 164.07, 169.77. Anal. Calc. for $C_{20}H_{15}IN_2O_2$: C, 54.32%; H, 3.42%; N, 6.33%. Found: C, 54.54%; H, 3.45%; N, 6.29%.

*4.1.7.9. N-(2-carbamoyl-4-chlorophenyl)-[1,1'-biphenyl]-4-carboxamide (**14c**).* 47% yield; mp 210–212 °C (ethanol); I.R. (KBr) cm^{-1} 3384-3216 (NH, NH_2), 1668, 1651 (2 CO) ^{1}H-NMR (DMSO) δ 7.43–8.77 (set of signals, 14H, aromatic protons and exchangeable NH_2); 12.95 (s, 1H, NH; exchangeable with D_2O). ^{13}C-NMR (δ) (DMSO) 120.72, 121.75, 126.43, 126.93, 127.14, 127.64, 128.27, 128.35, 129.05, 132.25, 133.01, 138.84, 138.97, 143.66, 164.09, 169.85. Anal. Calc. for $C_{20}H_{15}ClN_2O_2$: C, 68.48%; H, 4.31%; N, 7.99%. Found: C, 68.44%; H, 4.70%; N, 7.76%.

*4.1.7.10. N-(2-carbamoyl-4-methylphenyl)-[1,1'-biphenyl]-4-carboxamide (**14d**).* 44% yield; mp 220–222 °C (ethanol); I.R. (KBr) cm^{-1} 3424, 3321, 3113 (NH, NH_2), 1656, 1645 (2 CO) ^{1}H-NMR (DMSO) δ 2.32 (s, 3H, CH_3); 7.40–8.66 (set of signals, 14H, aromatic protons and exchangeable NH_2); 12.95 (s, 1H, NH; exchangeable with D_2O). ^{13}C-NMR (δ) (DMSO) 20.85, 119.52, 120.44, 127.37, 127.54, 128.03, 128.66, 129.50, 132.14, 133.47, 133.89, 138.17, 139.39, 143.87, 164.25, 171.72. Anal. Calc. for $C_{21}H_{18}N_2O_2$: C, 76.34%; H, 5.49%; N, 8.48%. Found: C, 76.22%; H, 5.26%; N, 8.18%.

*4.1.7.11. N-(2-carbamoyl-4-methoxyphenyl)-[1,1'-biphenyl]-4-carboxamide (**14e**).* 55% yield; mp 242–244 °C (ethanol); I.R. (KBr) cm^{-1} 3356, 3245, 3186 (NH, NH_2), 1655, 1645 (broad, 2 CO) ^{1}H-NMR (DMSO) δ 3.86 (s, 3H, OCH_3); 7.21–8.69 (set of signals, 14H, aromatic protons and exchangeable NH_2); 12.74 (s, 1H, NH; exchangeable with D_2O). ^{13}C-NMR (δ) (DMSO) 55.51, 113.58, 118.09, 120.59, 121.65, 126.89, 127.05, 127.50, 128.17, 129.03, 133.34, 133.48, 138.94, 143.30, 154.32, 163.56, 170.83. Anal. Calc. for $C_{21}H_{18}N_2O_3$: C, 72.82%; H, 5.24%; N, 8.09%. Found: C, 73.15%; H, 5.55%; N, 8.16%.

*4.1.7.12. N-(2-carbamoyl-4,5-dimethoxyphenyl)-[1,1'-biphenyl]-4-carboxamide (**14f**).* 53% yield; mp 230–232 °C (ethanol); I.R. (KBr) cm^{-1} 3356, 3245, 3186 (NH, NH_2), 1655, 1645 (broad, 2 CO) ^{1}H-NMR (DMSO) δ 3.84 (s, 3H, OCH_3); 3.87 (s, 3H, OCH_3); 7.43–8.57 (set of signals, 13H, aromatic protons and exchangeable NH_2); 13.43 (s, 1H, NH; exchangeable with D_2O). ^{13}C-NMR (δ) (DMSO) 55.45, 55.98, 103.93, 110.06, 111.76, 126.90, 127.08, 127.52, 128.19, 129.03, 133.51, 135.87, 138.92, 143.37, 143.60, 151.65, 163.76, 171.01. Anal. Calc. for $C_{22}H_{20}N_2O_4$: C, 70.20%; H, 5.36%; N, 7.44%. Found: C, 69.80%; H, 5.27%; N, 7.35%.

*4.1.7.13. N-(2-carbamoylphenyl)-[1,1'-biphenyl]-2-carboxamide (**17a**).* 28% yield; mp 155–163 °C (ethanol); I.R. (KBr) cm^{-1} 3375, 3197-2960 (NH, NH_2), 1668, 1622 (2 CO) ^{1}H-NMR (DMSO) δ 7.09–8.49 (set of signals, 15H, aromatic protons and exchangeable NH_2); 11.94 (s, 1H, NH; exchangeable with D_2O). ^{13}C-NMR (δ) (DMSO) 119.64, 120.00, 122.68, 127.34, 127.56, 127.74, 128.28, 128.36, 128.56, 130.34, 130.41, 132.24, 136.74, 139.49, 139.57, 139.81, 167.41, 170.51. Anal. Calc. for $C_{20}H_{16}N_2O_2$: C, 75.93%; H, 5.10%; N, 8.86%. Found: C, 75.80%; H, 5.44%; N, 9.03%.

*4.1.7.14. N-(2-carbamoyl-4-iodophenyl)-[1,1'-biphenyl]-2-carboxamide (**17b**).* 30% yield; mp 152–156 °C (ethanol); I.R. (KBr) cm^{-1} 3228, 3199, 3076 (NH, NH_2), 1659, 1655 (2 CO) ^{1}H-NMR (DMSO) δ 7.29–8.27 (set of signals, 14H, aromatic protons and exchangeable NH_2); 11.77 (s, 1H, NH; exchangeable with D_2O). ^{13}C-NMR (δ) (DMSO) 86.84, 122.25, 122.48, 127.85, 128.07, 128.22, 128.75, 128.80, 130.84, 130.96, 136.93, 137.04, 139.51, 139.92, 140.13, 141.04, 167.85, 169.38. Anal. Calc. for $C_{20}H_{15}IN_2O_2$: C, 54.32%; H, 3.42%; N, 6.33%. Found: C, 53.93%; H, 3.26%; N, 6.40%.

*4.1.7.15. N-(2-carbamoyl-4-chlorophenyl)-[1,1'-biphenyl]-2-carboxamide (**17c**).* 15% yield; mp 145–147 °C (ethanol); I.R. (KBr) cm^{-1} 3329-3150 (NH, NH_2), 1682, 1646 (2 CO) ^{1}H-NMR (DMSO) δ 7.37–8.48 (set of signals, 14H, aromatic protons and exchangeable NH_2); 11.78 (s, 1H, NH; exchangeable with D_2O). Anal. Calc. for $C_{20}H_{15}ClN_2O_2$: C, 68.48%; H, 4.31%; N, 7.99%. Found: C, 68.77%; H, 4.03%; N, 7.71%.

*4.1.7.16. N-(2-carbamoyl-4-methylphenyl)-[1,1'-biphenyl]-2-carboxamide (**17d**).* 30% yield; mp 148–150 °C (ethanol); I.R. (KBr) cm^{-1} 3342, 3159, 3059 (NH, NH_2), 1677, 1641 (2 CO) ^{1}H-NMR ($CDCl_3$) δ 2.24 (s, 3H, CH_3); 5.73 (s, broad, 1H, NH-H, exchangeable with D_2O); 6.19 (s, broad, 1H, NH-H, exchangeable with D_2O); 7.20–8.48 (set of signals, 12H, aromatic protons); 10.88 (s, 1H, NH; exchangeable with D_2O). ^{13}C-NMR (δ) (DMSO) 20.73, 119.43, 121.40, 127.38, 127.53, 127.66, 128.28, 128.34, 128.83, 130.33, 130.60, 132.50, 133.60, 136.58, 137.11, 140.09, 140.17, 168.40, 170.93. Anal. Calc. for $C_{21}H_{18}N_2O_2$: C, 76.34%; H, 5.49%; N, 8.48%. Found: C, 76.35%; H, 5.25%; N, 8.52%.

*4.1.7.17. N-(2-carbamoyl-4-methoxyphenyl)-[1,1'-biphenyl]-2-carboxamide (**17e**).* 86% yield; mp 145–148 °C (ethanol); I.R. (KBr) cm^{-1} 3328, 3173, 3156 (NH, NH_2), 1684, 1651 (broad, 2 CO) ^{1}H-NMR (DMSO) δ 3.77 (s, 3H, OCH_3); 7.07–8.33 (set of signals, 14H, aromatic protons and exchangeable NH_2); 11.51 (s, 1H, NH; exchangeable with D_2O). ^{13}C-NMR (δ) (DMSO) 55.94, 113.87, 118.12, 121.89, 122.21, 127.80, 128.01, 128.18, 128.75, 128.81, 130.67, 130.81, 133.11, 137.39, 139.86, 104.35, 154.87, 167.42, 170.53. Anal. Calc. for $C_{21}H_{18}N_2O_3$: C, 72.82%; H, 5.24%; N, 8.09%. Found: C, 73.08%; H, 5.13%; N, 7.98%.

*4.1.7.18. N-(2-carbamoyl-4,5-dimethoxyphenyl)-[1,1'-biphenyl]-2-carboxamide (**17f**).* 88% yield; mp 210–212 °C (ethanol); I.R. (KBr) cm^{-1} 3414, 3336, 3204, (NH, NH_2), 1668, 1621 (2 CO) ^{1}H-NMR (DMSO) δ 3.72 (s, 6H, 2 OCH_3); 7.33–8.25 (set of signals, 13H, aromatic protons and exchangeable NH_2); 12.29 (s, 1H, NH; exchangeable with D_2O). ^{13}C-NMR (δ) (DMSO) 55.90, 56.38, 103.70, 110.94, 112.07, 127.80, 128.05, 128.24, 128.76, 128.87, 130.73, 130.90, 135.70, 137.41, 139.83, 140.31, 144.03, 151.86, 167.64, 170.71. Anal. Calc. for $C_{22}H_{20}N_2O_4$: C, 70.20%; H, 5.36%; N, 7.44%. Found: C, 70.03%; H, 5.32%; N, 7.21%.

4.2. Biology

4.2.1. Cell culture

Human leukemia K562 cells and human colon carcinoma HT29 cells were grown in RPMI 1640 medium supplemented with 10% foetal bovine serum (FBS), 2 mM glutamine, 50 U/ml penicillin and 50 μg/ml streptomycin at 37 °C in a humidified atmosphere containing 5% CO_2. Human breast cancer MDA-MB231 cells and human normal bronchial epithelial 16HBE cells were grown as monolayer in DMEM supplemented with 10% (v/v) FCS, 2 mM glutamine and 1% non-essential amino acids at 37 °C in a humidified atmosphere containing 5% CO_2. Before each experiment cells were seeded in 96 or 6-well plates and were allowed to adhere and grow until 70% confluency when they were treated with drugs. Human leukemia K562 cells were seeded on poly-D-lysine coated plates. Compounds were solubilized in DMSO (10 mM) and diluted in culture medium to final concentration. In all experiments, DMSO never exceeded the final concentration of 0.5% (v/v) to avoid any related toxic effect.

4.2.2. MTT cell viability assay

For cell viability experiments, cells (6×10^3 cells/well) were seeded in poly-D-lysine coated 96 well plates and after 24 h were incubated with compounds. The cytotoxicities of all analyzed compounds were determined by MTT (3-(4,5-dimethylthiazol-2-yl-2,5-diphenyl tetrazolium bromide) cell viability assay (Sigma-Aldrich, Milan, Italy) as previously reported [25]. Briefly, 20 μl of MTT solution (11 mg/ml) were added to the cells and incubation was protracted for 2 h at 37 °C, then the reaction was stopped replacing the medium with 100 μl of lysis buffer (20% SDS, 10% dimethylformamide and 20% acetic acid). The absorbance was read at 570 and 690 nm. Each condition was assayed six times and reported results are the mean of three separate experiments. The percentage of viable cells was estimated relative to the control value (vehicle–incubated cells) which was taken as 100.

4.2.3. Flow cytometric analysis and Hoechst staining of cells

The analysis of cell cycle distribution was performed as previously described [26]. Briefly, 1.5×10^5 K562 cells/well were seeded in poly-D-lysine coated 6 well plates and treated for 24 and 48 h in the presence or absence of compounds. Then cells were harvested, washed in PBS and stained for 2 h with propidium iodide (50 μg/ml in PBS, containing 100 μg/ml RNase A). At the end cells were washed and subjected to flow cytometry analysis using Beckman Coulter Epics XL cytometer. All data were recorded and analyzed using Expo32 software.

To assess the degree of correlation between the percentage of fragmented DNA, detected by propidium iodide staining, and the extent of damaged DNA, visualized as DNA condensation or fragmentation, a Hoechst staining of nuclei was performed as previously reported [27]. Hoechst is a popular cell-permeant nuclear dye that emits blue fluorescence when bound to dsDNA. It is often used to distinguish condensed pyknotic nuclei in apoptotic cell. To this purpose, cells were incubated with 2.5 μg/ml Hoechst 33342 (Sigma-Aldrich, Milan, Italy) for 30 min at 37 °C, then compounds were added and the incubations were protracted for the indicated times. At the end cell morphology was visualized by a Leica DC 300F microscope (Leica microsystems, Wetzlar, Germany) using appropriate filters to examine Hoechst staining (DAPI filter with $\lambda_{ex} = 372$ nm and $\lambda_{em} = 456$ nm).

4.2.4. Western blotting analysis

Cell lysates were prepared and quantified by Bradford assay as previously reported [28,29]. Protein samples (30 μg/lane) were subjected to SDS polyacrylamide gel electrophoresis and then transferred to a nitrocellulose membrane for the detection with specific antibodies. Analyses of phospho-ATM, γH2AX, phospho-JNK and pro-caspase-3 were performed by using specific antibodies produced by Santa Cruz Biotechnology (Santa Cruz, CA), while antibody for β-tubulin was provided by Sigma Aldrich (Milan, Italy). Protein bands were detected by ECL Plus™ Western Blotting Reagents (Amersham, GE Healthcare Life Science, MI, Italy). The quantification of band intensity in immunoblot was performed by Image J software. Equal loading of proteins into the gel was verified by immunoblotting for β-tubulin. All the blots shown are representative of at least three separate experiments.

4.2.5. Detection of reactive oxygen species generation

The production of reactive oxygen species was determined using the oxidation of the cell-permeant 2′,7′-dichlorodihydrofluorescein diacetate (H2DCFDA) dye as previously reported [30]. For these experiments 8×10^3 cells/well were seeded in 96 well plates in RPMI medium supplemented with 10% FBS. After incubation with the compounds for the indicated times, cells were centrifuged 10 min at 800 rpm, washed once Hanks' Balanced Salt Solution in HEPES buffered salt solution (HBSS) and loaded with 100 μM H2DCFDA dye for 30 min in the dark in an incubator with 5% CO_2 at 37 °C. Then fluorochrome was removed, cells were washed in HBSS and analyzed by fluorescence microscopy by using excitation and emission wavelengths that are appropriate for green fluorescence (FITC filter with $\lambda_{ex} = 485$ nm and $\lambda_{em} = 530$ nm).

4.2.6. Statistical analysis

Data were analyzed using Student's t-test and were reported as means ± standard error.

Acknowledgement

Financial support from “Fondo di Finanziamento della Ricerca di Ateneo (ex 60%)” is gratefully acknowledged.

Appendix A. Supplementary data

Supplementary data related to this article can be found at http://dx.doi.org/10.1016/j.ejmech.2017.03.051. These data include MOL files and InChiKeys of the most important compounds described in this article.

Abbreviations

ATM, ataxia telangiectasia mutated; DMSO, dimethyl sulfoxide; HBSS, Hanks' Balanced Salt Solution; H2DCFDA, 2′,7'-dichlorodihydrofluorescein diacetate; JNK, c-Jun N-terminal kinase, MAPK, mitogen-activated protein kinase, PI, propidium iodide; ROS, reactive oxygen species.

References

[1] B. Maggio, D. Raffa, M.V. Raimondi, S. Cascioferro, M.L. Trincavelli, C. Martini, F. Meneghetti, L. Basile, S. Guccione, G. Daidone, Synthesis, benzodiazepine receptor binding and molecular modeling of isochromeno[4,3-c]pyrazol-5(1H)-one derivatives, Eur. J. Med. Chem. 54 (2012) 709–720.

[2] D. Raffa, O. Migliara, B. Maggio, F. Plescia, S. Cascioferro, M.G. Cusimano, G. Tringali, C. Cannizzaro, F. Plescia, Pyrazolobenzotriazinones derivatives as COX inhibitors: synthesis biological activity and molecular modeling studies, Arc. Pharm. 10 (2010) 631–638.

[3] M.V. Raimondi, B. Maggio, D. Raffa, F. Plescia, S. Cascioferro, G. Cancemi, D. Schillaci, M.G. Cusimano, M. Vitale, G. Daidone, Synthesis and antistaphylococcal activity of new 4-diazopyrazole derivatives, Eur. J. Med. Chem. 58 (2012) 64–71.

[4] B. Maggio, M. Raimondi, D. Raffa, F. Plescia, M. Scherrmann, N. Prosa, M. Lauricella, A. D'Anneo, G. Daidone, Synthesis and antiproliferative activity of a natural like glycoconjugate polycyclic compound, Eur. J. Med. Chem. 122 (2016) 247–256.

[5] B. Maggio, M.V. Raimondi, D. Raffa, F. Plescia, S. Cascioferro, S. Plescia, M. Tolomeo, A. Di Cristina, R.M. Pipitone, S. Grimaudo, G. Daidone, Synthesis of substituted 3-amino-N-phenyl-1H-indazole-1-carboxamides endowed with antiproliferative activity, Eur. J. Med. Chem. 46 (2011) 168–174.

[6] B. Maggio, D. Raffa, M.V. Raimondi, M.G. Cusimano, F. Plescia, S. Cascioferro, G. Cancemi, M. Lauricella, D. Carlisi, G. Daidone, Synthesis and antiproliferative activity of new derivatives containing the polycyclic system 5,7:7,13-dimethanopyrazolo[3,4-b]pyrazolo[3′,4′:2,3]azepino[4,5-F]azocine, Eur. J. Med. Chem. 72 (2014) 1–9.

[7] B. Maggio, M.V. Raimondi, D. Raffa, F. Plescia, S. Cascioferro, G. Cancemi, M. Tolomeo, S. Grimaudo, G. Daidone, Synthesis and antiproliferative activity of 3-(2-Chloroethyl)-5-Methyl-6-Phenyl-8-(Trifluoromethyl)-5,6-dihydropyrazolo[3,4-f][1,2,3,5]tetrazepin-4-(3H)-One, Eur. J. Med. Chem. 96 (2015) 98–104.

[8] D. Raffa, B. Maggio, S. Cascioferro, M.V. Raimondi, D. Schillaci, G. Gallo, G. Daidone, S. Plescia, F. Meneghetti, G. Bombieri, A. Di Cristina, R.M. Pipitone, S. Grimaudo, M. Tolomeo, Synthesis and antiproliferative activity of 3-amino-N-phenyl-1H-indazole-1-carboxamides, Eur. J. Med. Chem. 44 (2009) 165–178.

[9] D. Raffa, B. Maggio, S. Cascioferro, M.V. Raimondi, G. Daidone, S. Plescia, D. Schillaci, M.G. Cusimano, L. Titone, C. Colomba, M. Tolomeo, N-(indazolyl) benzamido derivatives as CDK1 inhibitors: design, synthesis, biological activity and molecular docking studies, Arch. Pharm. 342 (2009) 265–273.

[10] B. Maggio, D. Raffa, M.V. Raimondi, S. Cascioferro, F. Plescia, M. Tolomeo, E. Barbusca, G. Cannizzo, S. Mancuso, G. Daidone, Synthesis and induction of G0-G1 phase arrest with apoptosis of 3,5-dimethyl-6-phenyl-8-(trifluoromethyl)-5,6-dihydropyrazolo[3,4-f][1,2,3,5]tetrazepin-4(3H)-one, Eur. J. Med. Chem. 43 (2008) 2386–2394.

[11] D. Raffa, B. Maggio, F. Plescia, S. Cascioferro, S. Plescia, M.V. Raimondi, G. Daidone, M. Tolomeo, S. Grimaudo, A. Di Cristina, R.M. Pipitone, R. Bai, E. Hamel, Synthesis, antiproliferative activity, and mechanism of action of a series of 2-{[(2e)-3-phenylprop-2-enoyl]amino}benzamides, Eur. J. Med. Chem. 46 (2011) 2786–2796.

[12] D. Raffa, B. Maggio, M.V. Raimondi, M.G. Cusimano, G. Amico, A. Carollo, P.G. Conaldi, R. Bai, E. Hamel, G. Daidone, 2-Cinnamamido, 2-(3-phenylpropiolamido), and 2-(3-phenylpropanamido)benzamides: synthesis, antiproliferative activity, and mechanism of action, Eur. J. Med. Chem. 65 (2013) 427–435.

[13] D. Raffa, B. Maggio, F. Plescia, S. Cascioferro, M.V. Raimondi, G. Cancemi, A. D'Anneo, M. Lauricella, M.G. Cusimano, R. Bai, E. Hamel, G. Daidone, Synthesis, antiproliferative activity and possible mechanism of action of novel 2-acetamidobenzamides bearing the 2-phenoxy functionality, Bioorg. Med. Chem. 23 (2015) 6305–6316.

[14] M. H. Palmer, G. J. McVie, Alkylation and acylation reactions. Part II. The interaction of aryloxyacetyl chlorides with aluminium chloride journal of the chemical society B: physical organic (RSC publishing). J. Chem. Soc. B Phys. Org. 745–751.

[15] A. Balaban, T. Lexadru, A.M. Duffield, Derivatives od 2-biphenilcarboxylic acid, Révue Romaine Chim. 16 (1971) 1095–1098.

[16] T. Sardon, T. Cottin, J. Xu, A. Giannis, I. Vernos, Development and biological evaluation of a novel aurora a kinase inhibitor, ChemBioChem 10 (2009) 464–478.

[17] A.N. Kousholt, T. Menzel, C.S. Sorensen, Pathways for genome integrity in G2 phase of the cell cycle, Biomolcule 3 (2003) 72–74.

[18] D.H. Larsen, M. Stucki, Nucleolar responses to DNA double-strand breaks, Nucleic Acids Res. 44 (2016) 538–544.

[19] J. Filligham, M.-C. Keogh, N.J. Krogan, γH2AX and its role in DNA double-strand break repair, Biochem. Cell Biol. 84 (2006) 568–577.

[20] M.A. Kang, E.-Y. So, A.L. Simons, D.R. Spitz, T. Ouchi, DNA damage induces reactive oxygen species generation through the H2AX-Nox1/Rac1 pathway, Cell Death Dis. 3 (2012) e249.

[21] M.S. Cooke, Oxidative DNA damage: mechanisms, mutation, and disease, FASEB J. 17 (2003) 1195–1214.

[22] J.M. Matés, F.M. Sánchez-Jiménez, Role of reactive oxygen species in apoptosis: implications for cancer therapy, Int. J. Biochem. Cell Biol. 32 (2000) 157–170.

[23] Y. Shi, F. Nikulenkov, J. Zawacka-Pankau, H. Li, R. Gabdoulline, J. Xu, S. Eriksson, E. Hedström, N. Issaeva, A. Kel, E.S.J. Arnér, G. Selivanova, ROS-dependent activation of JNK converts p53 into an efficient inhibitor of oncogenes leading to robust apoptosis, Cell Death Differ. 21 (2014) 612–623.

[24] D.N. Dhanasekaran, E.P. Reddy, JNK signaling in apoptosis, Oncogene 27 (2008) 6245–6251.

[25] G. Calvaruso, M. Carabillo, M. Giuliano, M. Lauricella, A. D'Anneo, R. Vento, G. Tesoriere, Sodium phenylbutyrate induces apoptosis in human retinoblastoma Y79 cells: the effect of combined treatment with the topoisomerase I-Inhibitor topotecan, Int. J. Oncol. 18 (2001) 1233–1237.

[26] M. Lauricella, A. Ciraolo, D. Carlisi, R. Vento, G. Tesoriere, SAHA/TRAIL combination induces detachment and anoikis of MDA-MB231 and MCF-7 breast cancer cells, Biochimie 94 (2012) 287–299.

[27] D. Carlisi, M. Lauricella, A. D'Anneo, G. Buttitta, S. Emanuele, R. Di Fiore, R. Martinez, C. Rolfo, R. Vento, G. Tesoriere, The synergistic effect of SAHA and parthenolide in MDA-MB231 breast cancer cells, J. Cell. Physiol. 230 (2015) 1276–1289.

[28] M. Lauricella, D. Carlisi, M. Giuliano, G. Calvaruso, C. Cernigliaro, R. Vento, A. D'Anneo, The analysis of estrogen receptor-α positive breast cancer stem-like cells unveils a high expression of the serpin proteinase inhibitor PI-9: possible regulatory mechanisms, Int. J. Oncol. 49 (2016) 352–360.

[29] R. Di Fiore, A. Guercio, R. Puleio, P. Di Marco, R. Drago-Ferrante, A. D'Anneo, A. De Blasio, D. Carlisi, S. Di Bella, F. Pentimalli, I.M. Forte, A. Giordano, G. Tesoriere, R. Vento, Modeling human osteosarcoma in mice through 3AB-OS cancer stem cell xenografts, J. Cell. Biochem. 113 (2012) 3380–3392.

[30] A. D'Anneo, D. Carlisi, M. Lauricella, S. Emanuele, R. Di Fiore, R. Vento, G. Tesoriere, Parthenolide induces caspase-independent and AIF-mediated cell death in human osteosarcoma and melanoma cells, J. Cell. Physiol. 228 (2013) 952–967.